

Two Energy Scales and two Quasiparticle Dynamics in the Superconducting State of Underdoped Cuprates

M. Le Tacon, A. Sacuto

Laboratoire Matériaux et Phénomènes Quantiques (UMR 7162 CNRS),

Université Paris 7, 2 place Jussieu 75251 Paris, France and

Laboratoire de Physique du Solide, ESPCI,

10 rue Vauquelin 75231 Paris, France

A. Georges

Centre de Physique Théorique, Ecole Polytechnique, 91128 Palaiseau Cedex, France

G. Kotliar

Centre de Physique Théorique, Ecole Polytechnique,

91128 Palaiseau Cedex, France and

Serin Physics Laboratory, Rutgers University, USA

Y. Gallais

Departments of Physics and Applied Physics,

Columbia University New York, NY 10027, USA

D. Colson, A. Forget

Service de Physique de l'Etat Condensé,

CEA-Saclay, 91191 Gif-sur-Yvette, France

(Dated: May 22, 2018)

Abstract

The superconducting state of underdoped cuprates is often described in terms of a single energy-scale, associated with the maximum of the (d -wave) gap. Here, we report on electronic Raman scattering results, which show that the gap function in the underdoped regime is characterized by two energy scales, depending on doping in opposite manners. Their ratios to the maximum critical temperature are found to be universal in cuprates. Our experimental results also reveal two different quasiparticle dynamics in the underdoped superconducting state, associated with two regions of momentum space: nodal regions near the zeros of the gap and antinodal regions. While antinodal quasiparticles quickly loose coherence as doping is reduced, coherent nodal quasiparticles persist down to low doping levels. A theoretical analysis using a new sum-rule allows us to relate the low-frequency-dependence of the Raman response to the temperature-dependence of the superfluid density, both controlled by nodal excitations.

PACS numbers: 74.72.-h, 74.62.Dh, 78.30.-j

Understanding the origin of high temperature superconductivity in copper oxide based materials is one of the outstanding problems in modern condensed matter theory. Two decades of intensive theoretical and experimental work have revealed that this phenomenon takes place in various families of cuprates, all containing copper oxide layers separated by building blocks that provide a reservoir of carriers. The cuprates phase diagram is remarkably universal. When there is nominally one hole per copper in the copper oxygen planes the cuprates are in an insulating phase due to correlations known as a Mott insulator. As the number of charge carriers is increased, a process called doping, the cuprates turn into a *d*-wave superconductor.

The superconducting temperature has a dome like shape as a function of doping and cuprates exhibit two physically distinct regimes: i) the under-doped regime where the critical temperature T_c increases with doping, ii) an over-doped regime where T_c decreases with doping. They are separated by optimal doping where T_c reaches its maximum. There is now consensus that the "normal state" above the superconducting critical temperature in the under-doped and optimally doped regimes is far from being normal. In particular, a pseudo gap develops in the underdoped regime, corresponding to a partial suppression of spin and charge excitations. This phenomenon lies outside the standard theory of solids and manifests itself in all experiments, such as neutron scattering cross sections, nuclear magnetic resonance (NMR), magnetic susceptibility, specific heat, angle resolved photoemission spectroscopy (ARPES), optical conductivity, tunneling and Raman spectroscopies (for a review, see Ref. [1]).

In contrast, there is no consensus on whether the superconducting state in the underdoped regime, which emerges from the Mott insulating state, can be described by the standard BCS-Migdal-Eliashberg theory for a *d*-wave superconductor. In this article, we address this issue using Electronic Raman Spectroscopy(ERS). ERS is a powerful tool for probing quasi-particles of the superconducting state in selected parts of the momentum space namely the antinodal (ANR) and nodal (NR) regions where the amplitude of the superconducting gap reaches its maximum and vanishes respectively [2]. Here ERS is performed on $\text{HgBa}_2\text{CuO}_{4+\delta}$ (Hg-1201) one of the most simple structure which takes a pure tetragonal symmetry with only one copper oxide plane per unit cell. By a judicious choice of the laser excitation lines we have enhanced the ERS signal allowing a direct view of the electronic properties of this cuprate without invoking *ad hoc* phonon subtraction procedures usually used in cuprate systems.

Our results demonstrate that the superconducting state on the underdoped side is also not normal, and cannot be described within the standard *d*-wave BCS model. We show that a minimal description of this state requires two energy scales and two quasiparticle dynamics. One scale is associated with the nodal region, and decreases with decreasing doping, while the second is associated with the antinodal region, and increases with decreasing doping. Close to the nodes the quasiparticle spectral weight remains substantial even at low doping in contrast to the antinodes where it drastically decreases. As a consequence i) we show that the superconducting order parameter is controlled by two parameters (the slope of the gap function at the nodes and the antinodal gap maximum) instead of one as expected from a standard *d*-wave gap, ii) we find a strong momentum dependence of the quasiparticles spectral weight in the superconducting state of the underdoped regime, and iii) we finally establish, using a new Raman sum-rule, a simple relationship between the superfluid density and the low-energy Raman scattering associated with nodal physics, suggesting that the Fermi liquid renormalization of the current (vector quantity) and stress

tensor (which transforms as a product of currents) have similar doping dependence. Our new experimental results place strong constraints on current theories of the high temperature superconductivity phenomenon.

EXPERIMENTAL RESULTS

The ERS measurements (see Methods section for details) have been performed on selected, as-grown, Hg-1201 single crystals from several batches with different doping levels extending from the slightly over-doped (OD) to the underdoped (UD) regime: ($T_c = 92\text{K(OD)}$, 95K(OP) , 89K(UD) , 78K(UD) and 63K(UD)).

ERS is an energy probe, but also a momentum probe which allows us to select different parts of the Fermi surface by choosing combinations of incident and scattered light polarizations [2]. The NR and ANR have been explored using cross polarizations parallel to the Cu-O bond directions (B_{2g}) and at 45° from them (B_{1g}), respectively. All spectra have been corrected for the spectral response of the spectrometer and for the Bose-Einstein factor. They are thus proportional to the imaginary part of the Raman response function $\chi''(\omega)$.

Figure 1 displays the NR (B_{2g}) and ANR (B_{1g}) Raman response functions in both the normal and superconducting states of the Hg-1201 single crystals, at various doping levels. At optimal doping ($T_c=95$ K), the electronic Raman continua for both the ANR and NR exhibit a redistribution of spectral weight from energies lower than 400 cm^{-1} to higher energy, when going from the normal state to the superconducting state. This redistribution is more pronounced for the ANR than for the NR. At low energy (below 400 cm^{-1}), the ANR superconducting continuum exhibits a cubic frequency dependence with a well-marked superconducting pair breaking peak, indicated by an arrow on Fig.1, at a frequency $\hbar\omega_{AN} \simeq 505\text{ cm}^{-1}$ ($\simeq 8k_B T_c$). In contrast, the superconducting spectrum in the NR displays a linear frequency dependence up to 400 cm^{-1} , as well as a weaker signature of the pair-breaking peak (arrow) close to the same frequency $\hbar\omega_N \simeq \hbar\omega_{AN}$ than for the ANR spectrum (but with a half width at half maximum reduced approximately by a factor of two). The Raman response at optimal doping is thus characterized by a single energy scale $\hbar\omega_{AN} \simeq \hbar\omega_N$ associated with the pair-breaking peak, and all the features described above are consistent with those expected for a d -wave superconductor [3] with a maximum value Δ_m of the superconducting gap given by $2\Delta_m = \hbar\omega_{AN}$ (see below). Our results for one overdoped sample (spectra at the top of Fig. 1) can also be interpreted in terms of a single energy scale.

In contrast, as doping is decreased below the optimal one, the evolution of the Raman spectra in the superconducting phase becomes strikingly different in the ANR and in the NR. As the doping level (and T_c) is reduced, the characteristic energy of the antinodal peak (indicated by an arrow on the right pannel of Fig. 1) increases. Simultaneously, the intensity of this peak rapidly decreases as T_c decreases, and finally disappears in the vicinity of $T_c=78\text{K}$. In contrast, the characteristic energy scale of the spectrum in the NR (which we take to be the frequency ω_N of the maximum observed in $\chi''(\omega)$) follows T_c . Furthermore, contrarily to the antinodal peak, the nodal peak persists down to the lowest doping that we have studied ($T_c=63\text{K}$). We note that similar observations have been reported previously on other cuprate materials, such as $\text{Bi}_2\text{Sr}_2\text{CaCu}_2\text{O}_{8+\delta}$ (Bi-2212), $\text{Bi}_2\text{Sr}_{2-x}\text{La}_x\text{CuO}_{6+\delta}$ (Bi-2201), $\text{YBa}_2\text{Cu}_3\text{O}_{7-\delta}$ (Y-123) and $\text{La}_{2-x}\text{Sr}_x\text{CuO}_4$ (LSCO) [4, 5]. This demonstrates that the electronic Raman response in the underdoped regime involves two distinct energy scales, with opposite doping dependence. As discussed below, this is inconsistent with a simple

BCS d -wave description [3].

In order to substantiate further this point, we have plotted in Fig. 2 the characteristic ratios $\hbar\omega_{AN}/k_B T_c^{max}$ and $\hbar\omega_N/k_B T_c^{max}$ obtained for several different families of cuprates by different groups [4, 5, 6], as a function of doping at a fixed temperature well below T_c . The doping value p is inferred from T_c using Tallon's equation [7]: $1 - T_c/T_c^{max} = 82.6(p - 0.16)^2$, with T_c^{max} the critical temperature at optimal doping. Fig. 2 reveals that these ratios have a universal dependence on doping. For underdoped compounds, two distinct scales are present, with the two ratios behaving in opposite manners as a function of doping, while a unique energy scale and doping dependence is recovered at optimal doping and in the overdoped regime.

INCONSISTENCY WITH A SIMPLE BCS MODEL

Let us now analyze these results using the simplest possible framework, that of a BCS superconductor with a d -wave gap function of the form $\Delta_k = \Delta_m \cos(2\phi)$ (where ϕ is the angle associated with momentum \mathbf{k} on the Fermi surface). The Raman response would then read [3, 8]:

$$\chi''_{AN,N}(\omega) = \frac{2\pi N_F}{\omega} \left\langle \frac{(\gamma^{AN,N}(\phi))^2 \Delta_m^2 \cos^2(2\phi)}{\sqrt{\omega^2 - 4\Delta_m^2 \cos^2(2\phi)}} \right\rangle_{FS} \quad (1)$$

$\gamma^{AN,N}(\phi)$ is the Raman vertex associated with each polarization: $\gamma^{AN}(\phi) = \gamma_{B_{1g}} \cos(2\phi)$ while $\gamma^N(\phi) = \gamma_{B_{2g}} \sin(2\phi)$, and $\langle \dots \rangle_{FS}$ denotes a Fermi-surface average. This predicts a sharp pair-breaking peak (corresponding to a divergence of this expression) in the B_{1g} (ANR) geometry at $\omega = 2\Delta_m$, and a weaker singularity in the B_{2g} (NR) geometry at the same frequency scale (furthermore, within the simplest BCS formula above, the B_{2g} (NR) response displays a maximum at a somewhat lower energy than the peak in the B_{1g} (ANR) channel, but both are governed by one energy scale, that of the maximal gap Δ_m). This is roughly consistent with the experimental observations at optimal doping, but completely fails to account for the underdoped spectra (for which the observed peaks become clearly distinct in each polarization and have opposite doping dependence).

This clearly demonstrates that one or both of the following assumptions become invalid in the underdoped regime: i) non-interacting BCS quasiparticles ii) a gap function with the simple form $\Delta_k = \Delta_m \cos(2\phi)$ characterized by a single energy scale. Moving away from assumption i) requires taking into account, in the framework of the Landau theory of interacting quasiparticles, the spectral weight Z_k of these quasiparticles, in general smaller than one and k -dependent, as well as the Fermi-liquid vertex Λ_k describing the interaction of the quasiparticles with external perturbations. This leads to:

$$\chi''_{AN,N}(\omega) = \frac{2\pi N_F}{\omega} \left\langle \frac{(Z\Lambda)_k^2 (\gamma_k^{AN,N})^2 \Delta_k^2}{\sqrt{\omega^2 - 4\Delta_k^2}} \right\rangle_{FS} \quad (2)$$

in which a general gap-function has also been taken into account. This expression contains two unknown functions of momentum on the Fermi-surface however: $(Z\Lambda)_k$ and Δ_k , and constructing on this basis a phenomenological analysis (to which we shall come back later in this paper) requires further insight.

LOW-ENERGY NODAL EXCITATIONS, SUM-RULE AND RELATIONSHIP TO THE SUPERFLUID DENSITY

In order to gain such insight, we have focused on the low-energy part of the Raman spectra, which is controlled by the properties of the nodal quasiparticles. The B_{2g} geometry is particularly significant in this respect, since the largest low-energy response is obtained in this geometry and the NR is directly sampled. Figures 1 and 3 demonstrate that a linear dependence on frequency is found in this geometry, for several dependent doping levels. This is expected from the above formula, which yields: $\chi''_N(\omega \rightarrow 0) = \gamma_{B_{2g}}^2 \frac{\pi^2 N_F}{2v_\Delta} (Z\Lambda)_N^2 \omega + \dots$. In this expression, $v_\Delta = \frac{d\Delta}{d\phi}|_N$ is the slope of the gap function at the nodes, and $(Z\Lambda)_N$ is the value of $(Z\Lambda)_k$ at the node. Hence, a study of the doping-dependence of the slope of the nodal (B_{2g}) response, allows determining, in principle, the important parameter $\alpha = \frac{N_F}{v_\Delta} (Z\Lambda)_N^2$ associated with nodal physics.

In order to compare the slopes of samples with different doping levels however, the Raman spectra must be properly normalized. To achieve this goal, we have established a theoretical sum-rule for the Raman intensity of a weakly doped Mott insulator, which reads, at low doping levels p : $\int_0^\Omega \chi''(\omega) \omega d\omega = Cp$. We have derived this expression (see Methods section below) by starting from a one-band t-J model, in which case the upper cutoff Ω can be taken to infinity, and the constant C depends on the hopping amplitudes and exchange constant: $C(t, t', J)$. We expect this expression to be general for a weakly doped Mott insulator, provided the upper cutoff is taken to be of the order of the bare bandwidth and significantly lower than the scale U associated with the upper band. We have normalized the Raman B_{2g} data using this sum-rule for our own data on Hg-1201. This is shown in Fig. 3, and reveals that in the doping range of interest the slope is doping- independent. In order to point out the universality of this phenomena, we have applied the same Raman sum-rule to a number of spectra previously published in the literature for Y-123 and Bi-2212 [4, 5, 6, 9]. The results for the slope α as a function of doping are displayed on Fig. 4. It is seen that the slope is essentially doping-independent for all doping levels between optimal doping ($p=0.16$) down to $p=0.09$. For smaller doping levels, the Y-123 data (two data points available) suggest that α may end up decreasing at very low doping.

This doping-independence of the Raman B_{2g} (NR) slope over an extended range of doping levels is very reminiscent of the behavior of the slope of the linear term in the temperature-dependence of the penetration depth (or superfluid density) [10, 11]: $\rho_s(T) = \rho_s(0) - \beta T + \dots$. This quantity is also associated with the physics of nodal quasiparticles, and given by almost the same expression [12, 13] $\beta \propto \frac{N_F}{v_\Delta} (Z\Lambda_\rho)_N^2$, except for the fact that the Fermi liquid parameter Λ_ρ corresponds to a different angular-momentum channel than in the case of Raman. The comparison made in Fig. 4 between these two quantities shows excellent agreement, hence establishing a previously unforeseen relation between Raman and penetration depth measurements. We also note that very recent experiments [14] do suggest deviations from $\beta = \text{const.}$ at very low doping levels, in agreement with the two highly underdoped Y-123 data points in Fig. 4. As pointed out in Ref. [12], the independence of the slope β of the superfluid density upon doping, in an extended range, is a serious difficulty for the simplest (“vanilla”) version of RVB theory [15], in either its auxiliary boson [16] or wave function formulations [17] [18]. Our observations reveal a similar problem in connection with Raman scattering.

Having established the doping-(in)dependence of the $\alpha = \frac{N_F}{v_\Delta} (Z\Lambda)_N^2$ parameter associated with nodal physics, we can make further progress in disentangling the relative effects of i)

quasiparticle dynamics and ii) the form of the gap function on the Raman spectra. Let us first assume that the gap function has the simple form: $\Delta_k = \Delta_m \cos(2\phi)$ characterized by a single energy scale (the maximum gap), and such that $v_\Delta = 2\Delta_m$. Since the behavior of the ANR (B_{1g}) peak implies that Δ_m increases as doping is reduced (Fig. 2), the doping-independence of α would then imply that $(Z\Lambda)_N$ must correspondingly increase as p is reduced. This behavior is highly unlikely to apply for a doped Mott insulator, since it would correspond to a reinforcement of the quasiparticle spectral weight as doping is reduced. Furthermore, ARPES data and theory do suggest that the nodal quasiparticle spectral weight decreases as p is reduced [19, 20]. Hence, we are led to suspect that the slope of the gap at the nodal points, v_Δ , must decrease as the doping level is reduced (in order to keep α constant) and hence does not track the maximum gap Δ_m . This, of course, has far reaching consequences, namely: that a pure $\cos(2\phi)$ form does not hold in the underdoped regime, and that two energy scales characterize this regime (as already foreseen from the above analysis in Fig. 2). Indeed, this has been previously suggested from ARPES experiments [21, 22], indicating that the superconducting gap function may change from a “V-shape” to a “U-shape” as the doping level is reduced.

PHENOMENOLOGICAL DESCRIPTION

We now return to the general expression for the Raman response based on Fermi liquid considerations, and explore whether reasonable momentum- and doping-dependence of the two functions $Z\Lambda(\phi)$ and $\Delta(\phi)$ (associated respectively with quasiparticle physics and with the superconducting gap) can describe our data. We use the shape of the gap function (consistent with d -wave symmetry) proposed from ARPES data in Ref. [21]: $\Delta(\phi) = \Delta_m(B \cos 2\phi + (1 - B) \cos 6\phi)$, where $0 \leq B \leq 1$. This form is characterized by two scales: the (antinodal) maximum gap Δ_m and the nodal slope $v_\Delta = \Delta_m(8B - 6)$. In a first attempt, we have taken $Z\Lambda$ to be ϕ -independent (uniform along the Fermi surface). The parameters Δ_m and B were varied, as in Ref. [21], and the values of $Z\Lambda$ chosen such as to keep the ratio $(Z\Lambda)_N^2/v_\Delta$ constant, for consistency with our experimental observation on the doping- independence of the slope α . We found that the resulting spectra (not shown) could capture only part of our experimental observations: the B_{1g} peak does move to higher energy but does not loose intensity quickly enough, and the B_{2g} response becomes very flat as v_Δ/Δ_m is reduced, but its maximum does not clearly recede towards lower energy. Hence, a variation of $Z\Lambda(\phi)$ along the Fermi surface is clearly needed, which we have chosen as displayed in Fig. 5b (chosen again in such a way that $(Z\Lambda)_N^2/v_\Delta$ is kept constant). The four curves colors in Fig. 5 are meant to correspond, qualitatively, to the overdoped (BCS), optimally doped, slightly and strongly underdoped regimes. The resulting spectra are displayed in Figs. 5c-d for both B_{1g} and B_{2g} geometries. All the main qualitative aspects of our experimental observations are captured by this simple phenomenological model, namely: the opposite variation of the nodal and antinodal peaks with energy, the constant nodal slope, and the drastic suppression of the antinodal peak due to the incoherence of the antinodal quasiparticles (consistent with Fermi surface “arcs” [23]).

COMPARISON TO OTHER EXPERIMENTS

Finally, we discuss whether other experimental probes support the existence of two energy scales in the superconducting state of the underdoped cuprates.

Let us first note that the two basic building blocks of the phenomenological analysis developed above are consistent with available information from ARPES experiments. The leading edge in the ANR (corresponding to the higher energy scale) was shown to increase as the doping level is reduced [24]. Evidence for a second energy scale associated with the nodal region, and varying in an opposite manner with doping, has been suggested from ARPES in Refs. [21, 22], with a corresponding change of the gap function as discussed above. More extensive ARPES studies of the leading edge in the NR are clearly needed. ARPES also reveals that the (gapped) antinodal quasiparticles in the superconducting state quickly loose spectral weight and eventually become incoherent as doping is reduced [20, 25], while nodal quasiparticles loose spectral weight as doping is reduced but maintain coherence down to low doping levels [19, 20].

It was suggested from thermal conductivity measurements on Y-123 [26] that the nodal slope of the gap, v_Δ increases as the doping level is reduced, which would seem in contradiction with our observations. However, closer examination [27] reveals that only one data point is available in the doping range of interest here, and more experiments are clearly needed.

Tunneling, while not being a momentum-selective probe like Raman or ARPES, exhibits a set of distinct superconducting line shapes as a function of doping. The main peak in these spectra moves to higher energies as doping is reduced from optimal doping [28, 29] (as also seen from break-junction measurements [30, 31]), and at the same time broadens considerably. This is consistent with the behavior of the larger energy scale, and with the rapid loss of coherence of antinodal quasiparticles. Fourier transform tunneling has shown that antinodal decoherence is closely related to a local charge order, at least in surface [29]. This is consistent with the loss of the electronic Raman response which is sensitive to the charge dynamics. In contrast, the observation of quasiparticle interferences from tunneling [32] provides strong evidence for the coherence of nodal quasiparticles. There are also some recent indications that the lower energy scale might show up as a low-voltage shoulder in the tunneling spectra of underdoped samples [29]. There are also some previous indications in the literature that the lower energy scale shows up as the gap edge in the Andreev reflection spectra of underdoped samples [33].

CONCLUSION

In summary, electronic Raman scattering clearly demonstrates the existence of two distinct energy scales in the superconducting state of underdoped cuprates, depending on doping in opposite ways. Here, we have suggested that these two scales are associated with the nodal slope of the gap function, and its maximum, respectively. Correspondingly, our experiments reveal two different dynamical properties of the quasiparticles in these two regions. Hence, the dichotomy between the coherence of nodal quasiparticles and the incoherence of antinodal ones, which is well established in the normal state, persists in the superconducting state in the underdoped regime. A theoretical analysis using a new sum-rule reveals that the superconducting state cannot be described within the standard BCS-Migdal Eliashberg theory applied with a pure $(\cos k_x - \cos k_y)$ gap. We have also established a new relation between

the behavior of the low-energy Raman response and that of the temperature-dependence of the superfluid stiffness, both associated with nodal physics. All these observations emphasize the key importance of the momentum space differentiation between nodal and antinodal regions in both the normal and superconducting state in the proximity to the Mott transition. The physics of momentum space differentiation can have multiple origins and has been stressed early on by many authors[34, 35]. Modern theoretical approaches, such as cluster perturbation theory, functional renormalization groups, and cluster extensions of Dynamical Mean Field Theory have shown to be able to capture this physics in both the weak coupling and strong coupling regimes of the Hubbard model [37, 38, 39]. Our results provide further tests of these methods and should stimulate further development of these approaches, aiming in particular at a quantitative evaluation of the ERS response.

METHODS

Details of the experimental procedure

The Hg-1201 single crystals have been grown by the flux method. The detailed procedure of the crystal growth is described elsewhere [40]. The magnetically measured transition widths are less than 5K for all samples. The ERS experiments have been carried out using a triple grating spectrometer (JY-T64000) equipped with a nitrogen cooled CCD detector. The crystals were mounted in near-vacuum (10^{-6} mbar) on the cold finger of a liquid helium cryostat. Rotation of the crystal was achieved in situ. Red (1.9 eV) and Green (2.4 eV) excitation lines have been used for probing the ANR and NR Raman response functions, respectively, in order to magnify the ERS signal. It has been experimentally shown that resonance effects occur for these lines and are probably due to the matching of the excitation energies to the inter-band transitions of Hg-1201 [41]. The spectra presented here have been taken below (T = 10 K, corrected from laser heating), and above T_c (T = 100 K for 92K(OD), 95K(OP) and 89K(UD) crystals, and T = 89 K for 78K(UD) and 63K(UD) crystals).

Theoretical sum-rule

The absolute value of the Raman intensity in samples with different doping levels or composition is difficult to ascertain experimentally, because it depends on geometric factors which are hard to measure, such as the penetration volume of the electromagnetic field into the sample. To circumvent this problem, and to make contact with the physics of the Mott insulator, we use a sum rule to normalize the Raman intensity. In Ref. [42], such a sum rule was derived for the Hubbard model. This cannot be used to interpret our experiment however, because it involves the contribution of the Raman intensity from the upper Hubbard band, which cannot be determined experimentally since it occurs at energies where other interband transitions take place. For this reason, we have extended the method of Ref. [42] and derived a new low-energy sum rule for the B_{2g} Raman intensity, directly for the $t - J$ model (for which the upper Hubbard band has been projected out). This sum-rule relates the low energy Raman intensity to the expectation value of a composite operator:

$$\int d\omega \omega \chi''(\omega) = \frac{\pi}{2} \langle [M, [H, M^\dagger]] \rangle = \sum_{ijkl} \sum_{\alpha\cdots\delta'} T_{ijlm}^{\alpha\alpha'\cdots\delta\delta'} \langle X_{\alpha\alpha'}(i) X_{\beta\beta'}(j) X_{\gamma\gamma'}(l) X_{\delta\delta'}(m) \rangle$$

In this expression, $X_{\alpha\alpha'}(i)$ is the Hubbard operator at site i , and the Greek indices $\alpha \cdots \delta'$ run over the three possible atomic states $0, \uparrow, \downarrow$. M is the B_{2g} Raman operator (stress tensor) $M = \sum_{\mathbf{k}\sigma} \sin k_x \sin k_y X_{\sigma 0}(\mathbf{k}) X_{0\sigma}(\mathbf{k})$ and H is the $t - J$ Hamiltonain (containing a hopping term and a superexchange interaction). We have calculated the tensor $T_{ijlm}^{\alpha\alpha' \cdots \delta\delta'}$ appearing on the r.h.s of this equation. For a hopping term involving nearest (t) and next-nearest neighbor (t'), assuming unbroken spatial and time reversal symmetry, we have checked that all non-zero contributions involve at least two fermionic operators (i.e. $X_{\sigma 0}$ or $X_{0\sigma}$) living on different sites. In the absence of translational symmetry breaking contributions involving exactly two such operators are proportional to doping. We have checked this from an explicit evaluation using e.g. slave-boson or dynamical mean-field theories. Details will be published elsewhere. Hence, the B_{2g} Raman intensity for the $t - t' - J$ model reads: $\int_0^\infty d\omega \omega \chi''(\omega) = C(t, t', J) p + \cdots$ at low doping levels, justifying the normalisation used above. A similar observation follows from a different sum rule [43].

[1] Timusk, T. & Statt, B. W., The pseudogap in high-temperature superconductors: an experimental survey, *Rep. Prog. Phys.*, **62**, 61 (1999).

[2] Gallais, Y., Sacuto, A., Devreux, T. P. & Colson, D., *Phys. Rev. B* **71**, 012506(B) (2005).

[3] Devreux, T. P. & Einzel, D., Electronic Raman Scattering in superconductors as a probe of anisotropic electron pairing, *Phys. Rev. B* **51**, 16336 (1995).

[4] Venturini, F. *et al.*, Doping dependence of the electronic Raman spectra in cuprates, *Journ. Phys. Chem. Solids*, **63**, 2345 (2001).

[5] Sugai, S., Suzuki, H., Takayanagi, Y., Hosokawa, T. & Hayamizu, N., Carrier-density-dependent momentum shift of the coherent peak and the LO phonon mode in p-type high- T_c superconductors, *Phys. Rev. B* **68**, 184504 (2003).

[6] Chen, X. K. *et al.*, Electronic Raman scattering in underdoped $\text{YBa}_2\text{Cu}_3\text{O}_{6.5}$, *Phys. Rev. B* **56**, R513, (1997).

[7] Presland, M. R., Tallon, J. L., Buckley, R. G., Liu, R. S. & Flower, N. E., General trends in oxygen stoichiometry effects on T_c in Bi and Tl superconductors, *Physica C*, **176**, 95 (1991).

[8] Klein M. & Dierker, S. B., Theory of Raman scattering in superconductors, *Phys. Rev. B* **29**, 4976 (1984).

[9] Hewitt, K. C. & Irwin, J. C., Doping dependence of the superconducting gap in $\text{Bi}_2\text{Sr}_2\text{CaCu}_2\text{O}_{8-\delta}$, *Phys. Rev. B* **66**, 054516 (2002).

[10] Bonn, D. A. *et al.*, *Czech. J. Phys.* **46**, 3195-3202 (1996).

[11] Panagopoulos, C. & Xiang, T., Relationship between the Superconducting Energy Gap and the Critical Temperature in High- T_c Superconductors, *Phys. Rev. Lett.* **81**, 2336 (1998).

[12] Lee, P. A. & Wen, X. G., Unusual Superconducting State of Underdoped Cuprates, *Phys. Rev. Lett.* **78**, 4111 (1997).

[13] Durst, A. C. & Lee, P. A., Impurity-induced quasiparticle transport and universal-limit Wiedemann-Franz violation in d -wave superconductors, *Phys. Rev. B* **62**, 1270, (2000).

[14] Broun, D. M. *et al.* *cond-mat* 0509223.

[15] Anderson, P. W., The resonating valence bond state in La_2CuO_4 and superconductivity, *Science* **235**, 1196 (1987).

[16] Kotliar, G. The Superexchange Mechanism and d -wave Superconductivity: Kotliar G. & Liu, J., *Phys. Rev. B* **38**, 5142 (1988).

- [17] Gros, C., Superconductivity in correlated wave functions, *Phys. Rev. B* **38**, 931 (1998).
- [18] Anderson, P. W. *et al.*, The physics behind high-temperature superconducting cuprates: the plain vanilla version of RVB, *J. Phys.: Condens. Matter*, **16**, R755 (2004).
- [19] Yoshida, T. *et al.*, Metallic Behavior of Lightly Doped $\text{La}_{2-x}\text{Sr}_x\text{CuO}_4$ with a Fermi Surface Forming an Arc, *Phys. Rev. Lett.* **91**, 027001 (2003).
- [20] Shen, K. M. *et al.*, Nodal Quasiparticles and Antinodal Charge Ordering in $\text{Ca}_{2-x}\text{Na}_x\text{CuO}_2\text{Cl}_2$, *Science* **307**, 901 (2005).
- [21] Mésot, J. *et al.*, Superconducting Gap Anisotropy and Quasiparticle Interaction: A Doping Dependent Photoemission Study, *Phys. Rev. Lett.* **83**, 840 (1999).
- [22] Borisenko, S. V. *et al.*, Superconducting gap in the presence of bilayer splitting in underdoped $(\text{Pb},\text{Bi})_2\text{Sr}_2\text{CaCu}_2\text{O}_{8-\delta}$, *Phys. Rev. B* **66**, 140509(R) (2002).
- [23] Norman, M. R. *et al.*, Destruction of the Fermi surface in underdoped high- T_c superconductors, *Nature*, **392**, 157 (1998).
- [24] Feng, D. L. *et al.*, Signature of Superfluid Density in the Single-Particle Excitation Spectrum of $\text{Bi}_2\text{Sr}_2\text{CaCu}_2\text{O}_{8+\delta}$, *Science* **289**, 277, (2000).
- [25] Ding, H. *et al.*, Coherent Quasiparticle Weight and Its Connection to High- T_c Superconductivity from Angle-Resolved Photoemission, *Phys. Rev. Lett.* **87**, 227001 (2001).
- [26] Sutherland, M. *et al.*, Thermal conductivity across the phase diagram of cuprates: Low-energy quasiparticles and doping dependence of the superconducting gap, *Phys. Rev. B* **67**, 174520 (2003).
- [27] Taillefer, L., private communication.
- [28] McElroy, K. *et al.*, Relating atomic scale electronic phenomena to wave-like quasiparticle states in superconducting $\text{Bi}_2\text{Sr}_2\text{CaCu}_2\text{O}_{8+\delta}$, *Nature* **422**, 520 (2003).
- [29] McElroy, K. *et al.*, Coincidence of Checkerboard Charge Order and Antinodal State Decoherence in Strongly Underdoped Superconducting $\text{Bi}_2\text{Sr}_2\text{CaCu}_2\text{O}_{8+\delta}$, *Phys. Rev. Lett.* **94**, 197005 (2005).
- [30] Miyakawa, N., Guptasarma, P., Zasadzinski, J. F., Hinks, D. G. & Gray, K. E., Strong Dependence of the Superconducting Gap on Oxygen Doping from Tunneling Measurements on $\text{Bi}_2\text{Sr}_2\text{CaCu}_2\text{O}_{8-\delta}$, *Phys. Rev. Lett.* **80**, 157 (1998).
- [31] Miyakawa, N. *et al.*, Predominantly Superconducting Origin of Large Energy Gaps in Underdoped $\text{Bi}_2\text{Sr}_2\text{CaCu}_2\text{O}_{8-\delta}$ from tunneling spectroscopy, *Phys. Rev. Lett.* **83**, 1018 (1999).
- [32] Hoffman, J. E. *et al.*, Imaging Quasiparticle Interference in $\text{Bi}_2\text{Sr}_2\text{CaCu}_2\text{O}_{8+\delta}$, *Science* **297**, 1148 (2002)
- [33] Deutscher G., Coherence and single-particle excitations in the high-temperature superconductors, *Nature* **397**, 410 (1999).
- [34] Stojkovic, B. P. & Pines, D., Theory of the longitudinal and Hall conductivities of the cuprate superconductors, *Phys. Rev. B* **55**, 8576 (1997).
- [35] Ioffe, L. B. & Millis, A. J., Zone-diagonal-dominated transport in high- T_c cuprates, *Phys. Rev. B* **58**, 11631 (1998).
- [36] Honerkamp, C., Salmhofer, M., Furukawa, N. & Rice, T. M., Breakdown of the Landau-Fermi liquid in two dimensions due to umklapp scattering, *Phys. Rev. B* **63**, 035109 (2001).
- [37] Katanin, A. A. & Kampf, A. P., Quasiparticle Anisotropy and Pseudogap Formation from the Weak-Coupling Renormalization Group Point of View, *Phys. Rev. Lett.* **93**, 106406 (2004).
- [38] Civelli, M., Capone, M., Kancharla, S. S., Parcollet, O. & Kotliar, G., Dynamical Breakup of the Fermi Surface in a Doped Mott Insulator, *Phys. Rev. Lett.*, **95**, 106402 (2005).
- [39] Sénéchal, D. & Tremblay, A. M. S., Hot Spots and Pseudogaps for Hole- and Electron-Doped

High-Temperature Superconductors, *Phys. Rev. Lett.*, **92**, 126401 (2004).

[40] Bertinotti, A. *et al.*, Synthesis, crystal structure and magnetic properties of superconducting single crystals of $\text{HgBa}_2\text{CuO}_{4+\delta}$, *Physica C*, **268**, 257 (1996).

[41] Le Tacon, M., Sacuto, A. & Colson, D., Two Distinct Electronic Contributions in the Fully Symmetric Raman Response of High T_c Cuprates, *Phys. Rev. B* **71**, 100504(R) (2005).

[42] Freericks, J. K., Devereaux, T. P., Moraghebi, M. & Cooper, S. L., Optical Sum Rules that Relate to the Potential Energy of Strongly Correlated Systems, *Phys. Rev. Lett.*, **94**, 216401 (2005).

[43] Shastry, S. & Shraiman, B., Theory of Raman scattering in Mott-Hubbard systems, *Phys. Rev. Lett.*, **65**, 1068 (1990).

[44] DeWilde Y. *et al.*, Unusual Strong-Coupling Effects in the Tunneling Spectroscopy of Optimally Doped and Overdoped $\text{Bi}_2\text{Sr}_2\text{CaCu}_2\text{O}_{8-\delta}$, *Phys. Rev. Lett.* **80**, 153, (1998).

[45] Shen, Z.-X. *et al.*, Temperature-Induced Momentum-Dependent Spectral Weight Transfer in $\text{Bi}_2\text{Sr}_2\text{CaCu}_2\text{O}_{8-\delta}$, *Science* **280**, 259 (1998).

[46] Campuzano, J. C. *et al.*, Electronic Spectra and Their Relation to the (π, π) Collective Mode in High- T_c Superconductors, *Phys. Rev. Lett.* **83**, 3709 (1999).

ACKNOWLEDGEMENTS

We are grateful to: S. Biermann, N. Bontemps, S.V. Borisenko, P. Bourges, M. Cazayous, R. Combescot, G. Deutscher, T.P. Devereaux, K. McElroy, P. Monod, M. Norman, C. Panagopoulos, Z.-X. Shen, and L. Taillefer for useful discussions. This research was supported by CNRS, by Ecole Polytechnique and by the "Chaire Blaise Pascal de la Fondation de l'Ecole Normale Supérieure et de la région Ile de France".

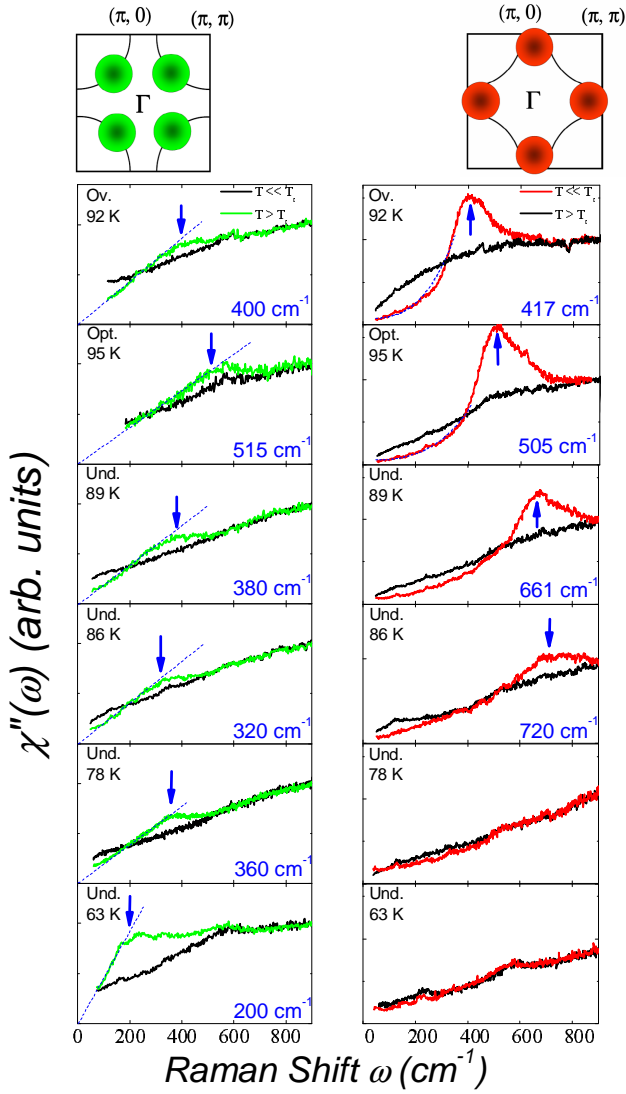


FIG. 1: Raman responses in the NR (B_{2g}) and ANR (B_{1g}) as function of doping. The dashed lines on (B_{2g}) (respectively (B_{1g})) spectra show the linear (resp. cubic) frequency dependences of the nodal (resp. antinodal) Raman responses. The arrows indicate the position of the superconducting peak maxima.

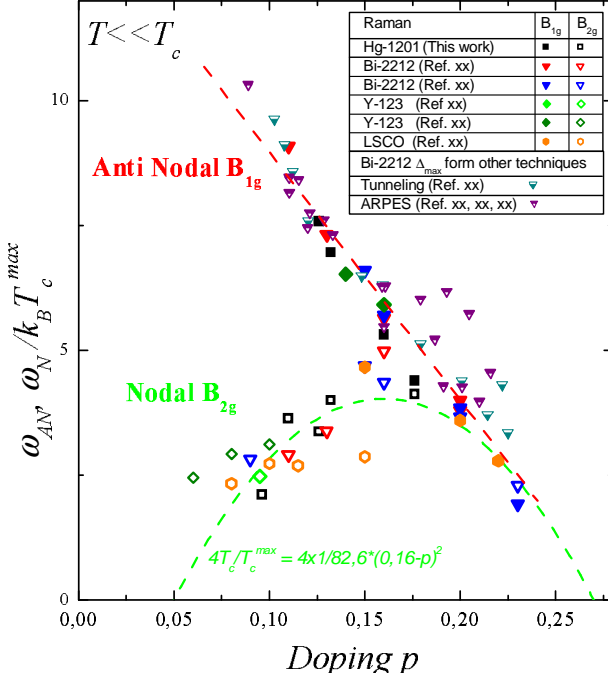


FIG. 2: Universal doping dependence of the ratios $\hbar\omega_{AN}/k_B T_c^{max}$ and $\hbar\omega_N/k_B T_c^{max}$ obtained from the B_{1g} and B_{2g} superconducting Raman peaks. The ratios $2\Delta/k_B T_c^{max}$ deduced from ARPES coherent peak in the ANR [23, 45, 46] and from tunneling spectroscopies [30, 31, 44] have also been reported.

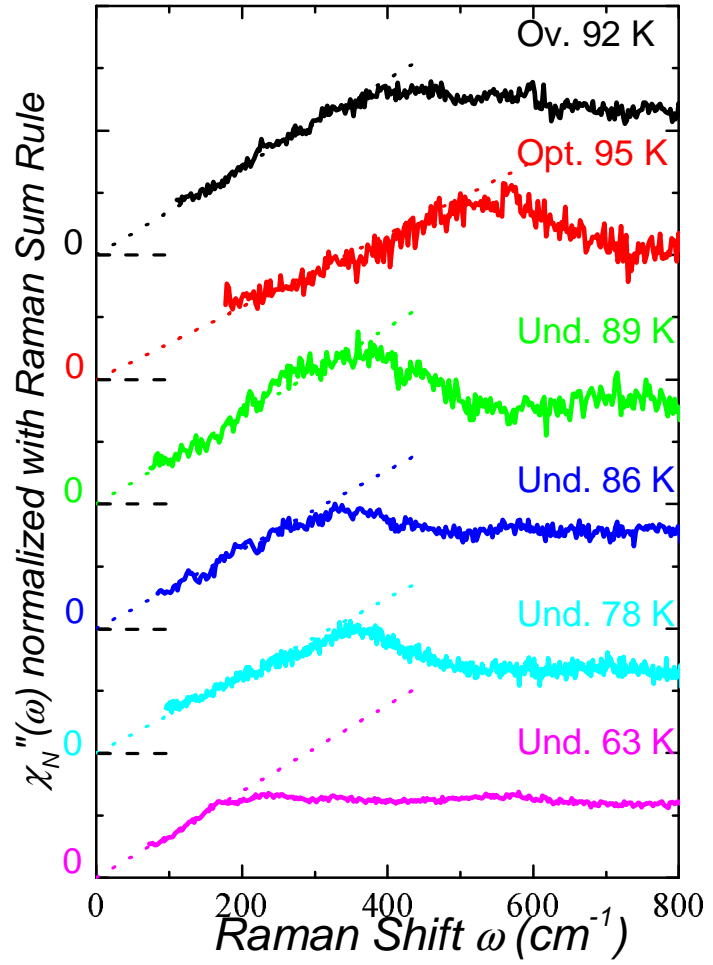


FIG. 3: Normalized Raman response functions with respect to the sum rule. A weak linear background coming from spurious luminescence for intermediate doping, independent of the scattering geometry and excitation lines has been subtracted from raw data before performing the normalization (note that without this subtraction the final result is qualitatively similar, i.e the low energy slopes of the normalized nodal Raman response are found to be doping independent).

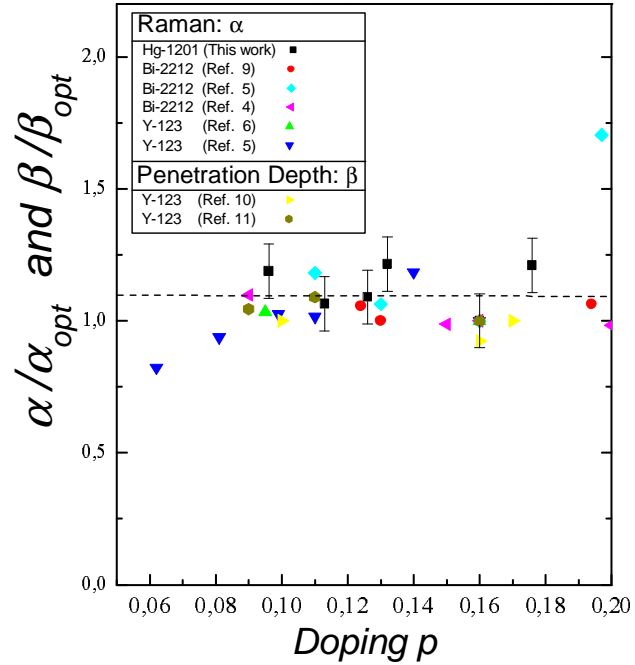


FIG. 4: Doping dependence of the slope of the nodal Raman response $\alpha = \frac{N_F}{v_\Delta} (Z\Lambda)_N^2$, normalized to the optimal doping one ($p = 0.16$). The Fermi liquid parameter $\beta = \frac{N_F}{v_\Delta} (Z\Lambda_\rho)_N^2$ extracted from the temperature dependence of the penetration depth [10, 11], is also shown. α and β are both found to be doping independent in the range ($p = 0.09 - 0.020$).

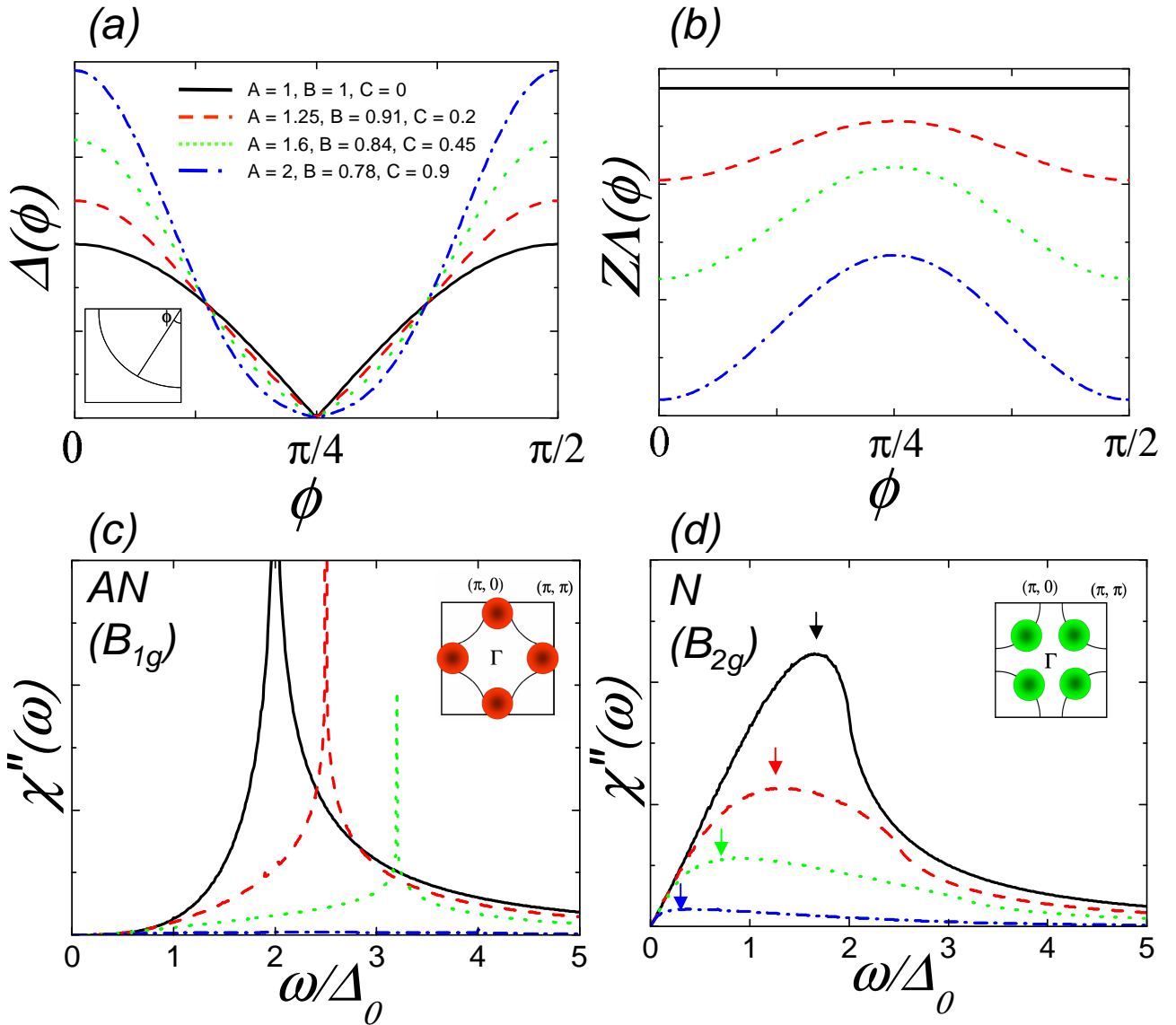


FIG. 5: (a) Momentum dependence of the phenomenological superconducting gap function: $\Delta(\phi) = A \times \Delta_0(B \cos 2\phi + (1 - B) \cos 6\phi)$. A is related to the maximum amplitude of the superconducting gap, and B to its deviation to the pure d -wave. (b) Momentum dependence of the phenomenological $Z\Lambda$ function: $Z\Lambda(\phi) = \sqrt{v_\Delta} \times (1 - C \cos^2(2\phi))$, where $v_\Delta = \frac{d\Delta}{d\phi}|_{\phi=\frac{\pi}{4}} = \Delta_m(8B - 6)$. (c) Calculated ANR (B_{1g}) response. (d) Calculated NR (B_{2g}) response function. Arrows indicate the position of the maximum.